Triplet Waves in a Quantum Spin Liquid

Guangyong Xu,[1] C. Broholm,[1,2] Daniel H. Reich,[1] and M. A. Adams[3]
[1]*Department of Physics and Astronomy, The Johns Hopkins University, Baltimore, Maryland 21218*
[2]*NIST Center for Neutron Research, National Institute of Standards and Technology, Gaithersburg, Maryland 20899*
[3]*ISIS Facility, CCLRC, RAL, Chilton, Didcot, Oxon, OX11 0QX, United Kingdom*
(Received 13 August 1999)

We report a neutron scattering study of the spin-1/2 alternating bond antiferromagnet $Cu(NO_3)_2 \cdot 2.5D_2O$ for $0.06 < k_BT/J_1 < 1.5$. For $k_BT/J_1 \ll 1$ the excitation spectrum is dominated by a coherent singlet-triplet mode centered at $J_1 = 0.442(2)$ meV with sinusoidal dispersion and a bandwidth of $J_2 = 0.106(2)$ meV. A complete description of the zero temperature contribution to the scattering function from this mode is provided by the single mode approximation. At finite temperatures we observe exponentially activated band narrowing and damping. The relaxation rate is thermally activated and wave vector dependent with the periodicity of the reciprocal lattice.

PACS numbers: 75.10.Jm, 75.40.Gb, 75.50.Ee, 78.70.Nx

Transverse phonons and spin waves are propagating small amplitude oscillations of a static order parameter in a broken symmetry phase. Isotropic quantum antiferromagnets with a gap in their excitation spectra can also support coherent wavelike excitations, but these differ from phonons and spin waves in that they move through a system with no static order. Specific examples of such systems include the spin-1 chain [1], even-leg ladders [2], and the alternating bond spin-1/2 chain [3–5]. Since they are not based on the existence of a static order parameter that sets in at a well defined transition temperature, coherent excitations in these systems are expected to emerge smoothly with decreasing temperature as short-range correlations develop.

In this Letter we document this unique cooperative behavior through an experimental study of the temperature dependence of magnetic excitations in an isotropic, order-parameter-free quantum magnet. Specifically, we have studied magnetic excitations in the alternating spin-1/2 chain copper nitrate (CN) as a function of wave vector, energy, and temperature. The spin Hamiltonian for this system can be written [3,4]

$$\mathcal{H} = \sum_n (J_1 \mathbf{S}_{2n} \cdot \mathbf{S}_{2n+1} + J_2 \mathbf{S}_{2n+1} \cdot \mathbf{S}_{2n+2}). \quad (1)$$

Because $J_2/J_1 \approx 0.24$ is small [4,6,7], it is useful to think of CN as a chain of pairs of spins-1/2. Each pair has a singlet ground state separated from a triplet at $J_1 \approx 0.44$ meV. The weak interdimer coupling ($J_2 \approx 0.11$ meV) yields a collective singlet ground state at low temperatures with triplet excitations that propagate coherently along the chain. We have characterized dynamic spin correlations in the temperature range $0.06 < k_BT/J_1 < 1.5$, in considerable detail. We find that heating yields thermally activated band narrowing and an increased relaxation rate that varies with wave vector transfer with the periodicity of the reciprocal lattice.

CN [$Cu(NO_3)_2 \cdot 2.5D_2O$] is monoclinic [8] (space group $I12/c1$) with low T lattice parameters $a = 16.1$ Å, $b = 4.9$ Å, $c = 15.8$ Å, and $\beta = 92.9°$. The vector connecting dimers center to center is $\mathbf{u}_0 = [111]/2$ for half the chains, and $\mathbf{u}_0' = [1\bar{1}1]/2$ for the other half. The corresponding intradimer vectors are $\mathbf{d}_1 = [0.252, \pm 0.027, 0.228]$, respectively. In our experiment, the wave vector transfer $\mathbf{Q}$ was perpendicular to $\mathbf{b}$ so the two sets of chains contributed equally to magnetic neutron scattering. The sample consisted of four 92% deuterated, co-aligned single crystals with total mass 14.09 g [9].

Inelastic neutron scattering measurements were performed on the inverse geometry time of flight spectrometer IRIS at the Rutherford Appleton Laboratory, U.K. [10]. Disk choppers selected an incident spectrum from 1.65 to 3.25 meV pulsed at 50 Hz, and a backscattering pyrolytic graphite analyzer bank selected a final energy $E_f = 1.847$ meV. The half width at half maximum (HWHM) elastic energy resolution was 10.5 μeV. The $\mathbf{b}$ direction of CN was perpendicular to the horizontal scattering plane and [101] pointed towards the low angle part of the analyzer bank at an angle of $\phi = 20(1)°$ to the direct beam. The direction for rotation of the $\mathbf{a}$ axis into the $\mathbf{c}$ axis coincided with the direction of decreasing scattering angle. In this configuration the projection of wave vector transfer on the chain $Q_\parallel = k_i \cos\phi - k_f \cos(2\theta - \phi)$ takes on a unique value for each detector in the range of scattering angles $20° < 2\theta < 160°$ covered. We can therefore present the measured neutron scattering intensity as a function of energy transfer $\hbar\omega$ and wave vector transfer along the chain $\tilde{q} = \mathbf{Q} \cdot \mathbf{u}_0$. Because there is a specific value of $Q_\perp = k_i \sin\phi + k_f \sin(2\theta - \phi)$ associated with each $(\tilde{q}, \hbar\omega)$ point, sensitivity to dispersion perpendicular to the chain is maintained in this projection. Count rates were normalized to incoherent elastic scattering from the sample to provide absolute measurements of $\tilde{I}(\mathbf{Q}, \omega) = |\frac{g}{2} F(Q)|^2 2S(\mathbf{Q}, \omega)$. Here $g = \sqrt{(g_b^2 + g_\perp^2)/2} = 2.22$ [4], $F(Q)$ is the magnetic form

factor for Cu^{2+} [11], and $S(\mathbf{Q},\omega)$ is the scattering function [12].

Figures 1(a)–1(c) show the measured neutron scattering intensity $\tilde{I}(\mathbf{Q},\omega)$ at $T = 0.3$, 2, and 4 K. Focusing at first on the 0.3 K data, we observe a resonant mode centered around $J_1 = 0.44$ meV with bandwidth $\approx J_2$, consistent with the predictions of perturbation theory [13]. The mode energy has the periodicity 2π of the one-dimensional reciprocal lattice with minima for $\tilde{q} = \mathbf{Q}\cdot\mathbf{u_0} = n\cdot 2\pi$, indicating antiferromagnetic interdimer interactions. The intensity of the mode varies with a periodicity that is incommensurate with that of the dispersion relation. There is a simple explanation for this, namely that the intradimer spacing that enters in the neutron scattering cross section is incommensurate with the period of the alternating spin chain [14]. An exact sum rule for $S(\mathbf{Q},\omega)$ provides the following direct link between the microscopic structure and the intensity of inelastic neutron scattering [15]:

$$\hbar\langle\omega\rangle_{\mathbf{Q}} \equiv \hbar^2\int_{-\infty}^{\infty}\omega S(\mathbf{Q},\omega)\,d\omega = -\frac{1}{3}\sum_{\mathbf{d}} J_{\mathbf{d}}\langle\mathbf{S}_0\cdot\mathbf{S}_{\mathbf{d}}\rangle(1-\cos\mathbf{Q}\cdot\mathbf{d}), \quad (2)$$

where $\{\mathbf{d}\}$ is the set of all bond vectors connecting a spin to its neighbors and $S(\mathbf{Q},\omega)$ is single site normalized. Figure 2(a) shows $\hbar\langle\omega\rangle_{\mathbf{Q}}$ at $T = 0.3$ and 4 K derived by integrating the corresponding data sets in Fig. 1. The solid lines show fits based on Eq. (2) including only intradimer correlations and a constant to account for multiple scattering (see below). The excellent agreement between model and data provides direct evidence for singlet formation between spins separated by $\mathbf{d}_1$. The modulation amplitude $J_1\langle\mathbf{S_0}\cdot\mathbf{S_{d_1}}\rangle/3$ is 0.16(3) meV and 0.06(1) meV at $T = 0.3$ and 4 K, respectively.

From the wave vector dependence of energy integrated intensities we turn to spectra at fixed wave vector transfer. Figure 3 shows cuts through raw data for $\tilde{q} = 2\pi$ and $\tilde{q} = 3\pi$ at three temperatures. At $T = 0.3$ K we see resolution limited peaks. Upon increasing temperature these peaks broaden and shift towards the center of the band. Careful inspection also reveals that the higher energy peak at $\tilde{q} = 3\pi$ broadens less than the lower energy peak at $\tilde{q} = 2\pi$. From Gaussian fits to constant energy cuts such as these, we extract the resonance energy and half width at half maximum versus wave vector transfer shown in Figs. 2(b) and 2(c). This analysis shows that the finite T relaxation rate is wave vector dependent with the apparent periodicity of the reciprocal lattice.

We now proceed to extract the detailed temperature dependence of the integrated intensity, the effective bandwidth and the relaxation rate. To take full advantage of

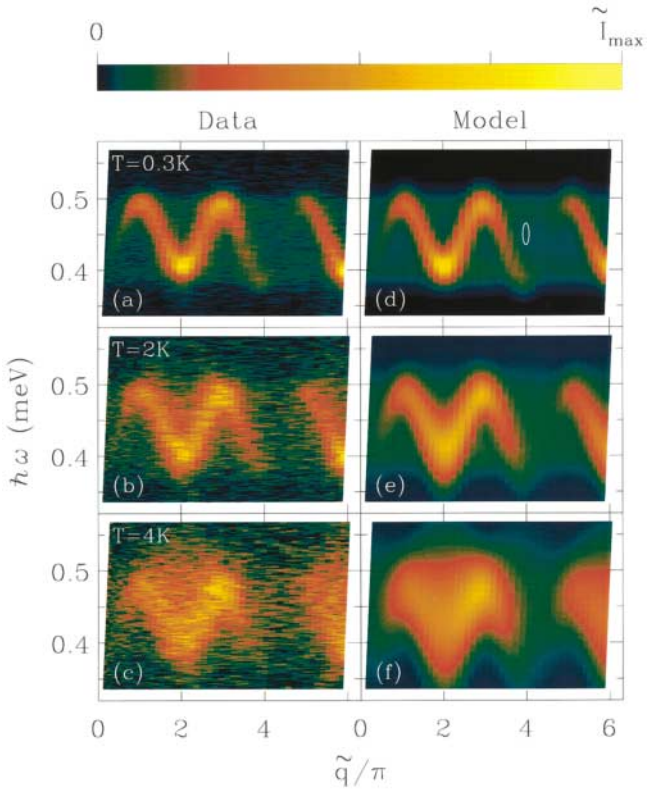

FIG. 1 (color). Normalized scattering intensity, $\tilde{I}(\tilde{q},\omega)$, for $Cu(NO_3)_2\cdot 2.5D_2O$ at (a) $T = 0.3$ K, (b) $T = 2$ K, and (c) $T = 4$ K. Maximum intensities on the color scale shown above are $\tilde{I}_{max} = 28, 16$, and 8 meV^{-1} per Cu, respectively. (d)–(f) show model calculations based on Eq. (3). The ellipse indicates the full width at half maximum resolution.

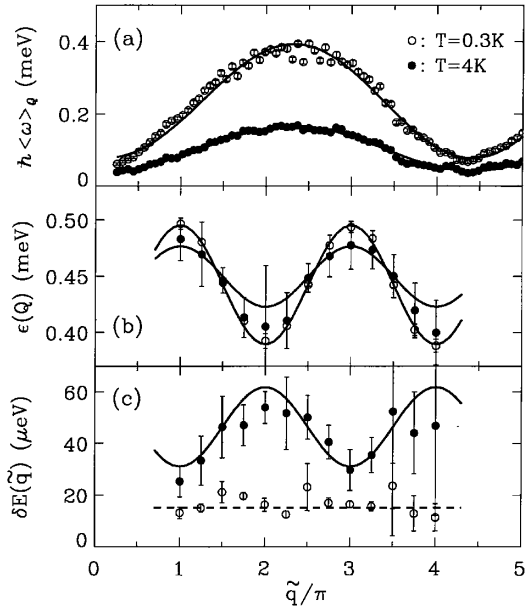

FIG. 2. First moment computed from Figs. 1(a) and 1(c) using (a) $\hbar\langle\omega\rangle_{\mathbf{Q}} = \hbar^2\int_0^{\infty}\omega(1-e^{-\beta\hbar\omega})S(\mathbf{Q},\omega)\,d\omega$, (b) resonance energy, and (c) HWHM $\delta E(\tilde{q})$ of the triplet mode in copper nitrate at $T = 0.3$ and 4 K. The points in (b) and (c) were obtained from fits to constant-$\tilde{q}$ cuts through the data in Fig. 1. The dashed line in (c) shows the HWHM instrumental energy resolution at $\hbar\omega = 0.45$ meV. The solid lines were obtained from fits described in the text.

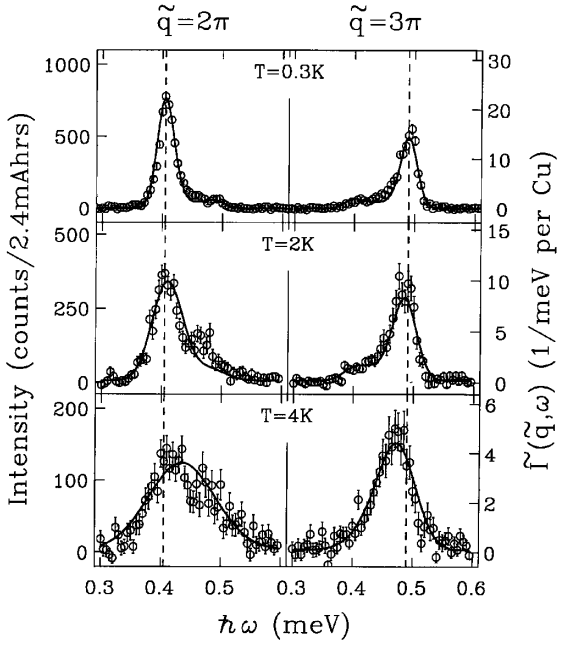

FIG. 3. Constant-$\tilde{q}$ cuts through the data shown in Fig. 1 at $\tilde{q} = 2\pi$ and 3π. The solid lines are the results of global fits at each T. The dashed lines indicate peak positions at $T = 0.3$ K, and highlight band narrowing at higher T.

the wide sampling of $\mathbf{Q} - \omega$ space in our experiment and to account for resolution effects, the analysis is based on "global fits" of the following phenomenological form for $S(\mathbf{Q}, \omega)$ to the complete $\mathbf{Q}$ and ω dependent data set at each temperature. For $\hbar\omega > 0$ we write

$$S(\mathbf{Q}, \omega) = \frac{\hbar\langle\omega\rangle_{\mathbf{Q}}}{\epsilon(\mathbf{Q})} \frac{1}{1 - \exp[-\beta\epsilon(\mathbf{Q})]} f[\hbar\omega - \epsilon(\mathbf{Q})], \tag{3}$$

where $f(E)$ is a normalized spectral function. The other terms implement the first moment sum rule of Eq. (2) when $f(E)$ is sharply peaked on the scale of J_1. Equation (3) represents the "single mode approximation" (SMA) that has been used with success to link the equal time structure factor and the dispersion relation for collective modes in numerous many body systems [15–17]. Given that two magnon scattering carries less than 1% of the spectral weight for CN [18], the SMA should be excellent at sufficiently low T. For the dispersion relation we use the following variational form based on first order perturbation theory [13]:

$$\epsilon(\mathbf{Q}) = J_1 - \frac{1}{2} \sum_{\mathbf{u}} J_{\mathbf{u}} \cos\mathbf{Q} \cdot \mathbf{u}\,. \tag{4}$$

The vectors $\{\mathbf{u}\}$ connect neighboring dimers center to center, both within and between the chains. For comparing to the experimental data, $S(\mathbf{Q}, \omega)$ was convolved with the instrumental resolution [10]. In all fits it was necessary to take into account multiple neutron scattering events involving elastic incoherent nuclear scattering followed or preceded by coherent inelastic magnetic scattering. We believe that such processes are responsible for the weak horizontal band of intensity that is visible in Fig. 1(a). For $T = 0.3$ K we used $f(E) = \delta(E)$ and obtained the fit shown in Fig. 1(d). To better evaluate the quality of the global fit we also show cuts through the model calculation as solid lines in Fig. 3. There is excellent agreement between model and data with an overall prefactor and four exchange constants in Eq. (4) as the only fit parameters. The prefactor refined to $\langle S_0 \cdot S_{\mathbf{d}_1}\rangle = -0.9(2)$ consistent with the value of $-3/4$ expected for isolated singlets. Allowing for interdimer correlations by including the corresponding term from Eq. (2) in the global fit yields $\langle \mathbf{S}_0 \cdot \mathbf{S}_{\mathbf{d}_2}\rangle = -0.04(8)$. The parameters in Eq. (4) refined to $J_1 = 0.442(2)$ meV and $J_2 = 0.106(2)$ meV for the two intrachain terms and $J_L = 0.012(2)$ meV and $J_R = 0.018(2)$ meV for dimers separated by $\mathbf{u}_L = [\frac{1}{2}, 0, 0]$ and $\mathbf{u}_R = [0, 0, \frac{1}{2}]$, respectively. Because $\mathbf{b} \perp Q$ throughout the experiment our data do not yield an estimate for interchain interactions between dimers displaced by $[1 \mp 11]/2$. However, in a separate measurement with the crystal oriented in the (hkh) plane [19], we were able to place an upper limit of 0.02 meV on the corresponding parameter in Eq. (4). The value $J_2/J_1 = 0.240(5)$ that we obtain is measurably smaller than the value $J_2/J_1 \approx 0.27$ [4] derived from magnetic susceptibility data. A likely explanation for this discrepancy is that susceptibility measurements cannot distinguish intrachain from interchain interactions.

To analyze the finite T data we replaced the spectral function with a normalized Gaussian with HWHM,

$$\Gamma(\tilde{q}) = \Gamma_0 + \frac{\Gamma_1}{2} \cos\tilde{q}\,. \tag{5}$$

The functional form for the dispersion relation [Eq. (4)] was maintained, but to account for the bandwidth narrowing that is apparent in the raw data, we introduced an overall renormalization parameter relating finite T "effective" exchange constants in the variational dispersion relation to the bare temperature independent exchange parameters: $\tilde{J}_{\mathbf{u}} = n(T)J_{\mathbf{u}}$. The fits obtained are excellent as can be ascertained by comparing the left and right columns in Fig. 1 and the solid lines through the data in Fig. 3. The solid lines in Figs. 2(b) and 2(c) show the dispersion relation and $\tilde{q}$-dependent relaxation rate derived from the global fits. They are consistent with the data points derived from constant-$\tilde{q}$ cuts indicating that the variational forms employed for $\epsilon(\tilde{q})$ and $\Gamma(\tilde{q})$ have not biased the global fitting analysis. We note that the quality of the fits did not change significantly when using a Lorentzian rather than a Gaussian spectral function. So while the data provide reliable information on the $\tilde{q}$- and T-dependent relaxation rate, they do not accurately determine the spectral function.

The temperature-dependent parameters derived from this analysis are shown in Fig. 4. The prefactor for global fits at each temperature yields the intradimer spin correlation function, which we plot versus T in Fig. 4(a). As expected $|\langle \mathbf{S}_0 \cdot \mathbf{S}_{\mathbf{d}_1}\rangle|$ decreases with increasing T as the

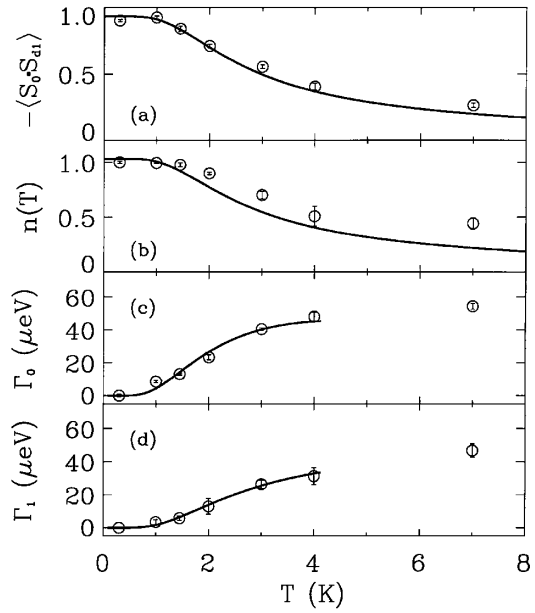

FIG. 4. Parameters characterizing the temperature dependence of dynamic spin correlations in CN, obtained from fits shown in Figs. 1 and 3. The solid lines in (a) and (b) show RPA theory. The solid lines in (c) and (d) are fits to $\Gamma_i(T) = \gamma_i(J_1/k_BT)^{\alpha_i}\exp(-J_1/k_BT)$.

populations of the four states of each spin pair equalize. For an isolated spin pair $\langle \mathbf{S}_0 \cdot \mathbf{S_d}\rangle = -(3/4)\Delta n(\beta J_1)$, where $\Delta n(\beta J_1) = (1 - e^{-\beta J_1})/(1 + 3e^{-\beta J_1})$ is the singlet-triplet population difference. After fitting a scale factor, this form provides an excellent description of the temperature dependence of the data [solid line in Fig. 4(a)]. The random phase approximation (RPA) applied to interacting spin dimers [20–23] predicts that the bandwidth renormalization factor, $n(T)$, also follows the singlet-triplet population difference. A similar result holds when the singlet ground state is induced by single ion anisotropy [24]. We compare $n(T)$ to $\Delta n(\beta J_1)$ in Fig. 4(b). While there is qualitative agreement, the RPA predicts significantly more bandwidth narrowing than observed.

Triplet relaxation is due to scattering from the thermal ensemble of excited states. Because the density of triplets is thermally activated, the relaxation rates should be too. Fits of a simple activated form $\Gamma_i = \gamma_i \exp(-\Delta_i/k_BT)$ to the $T \leq 4$ K data in Figs. 4(c) and 4(d) give $\Delta_0 = 0.24(2)$, $\gamma_0 = 0.10(2)$ meV, $\Delta_1 = 0.32(3)$, and $\gamma_1 = 0.08(2)$ meV. If we instead fix $\Delta_i \equiv J_1$ and allow for a power law prefactor: $\Gamma_i(T) = \gamma_i(J_1/k_BT)^{\alpha_i}\exp(-J_1/k_BT)$ we also obtain excellent fits with $\alpha_0 = 1.0(2)$, $\gamma_0 = 0.13(4)$ meV, $\alpha_1 = 0.6(2)$, and $\gamma_1 = 0.10(1)$ meV.

In summary, we have examined dynamic spin correlations in the strongly alternating spin chain $Cu(NO_3)_2 \cdot 2.5D_2O$ for $0.06 < k_BT/J_1 < 1.5$. For $k_BT \ll J_1$ we find a coherent dispersive triplet mode whose contribution to the scattering function is perfectly accounted for by the SMA, and we have determined accurate values for interdimer interactions in the material. Upon heating, the sharp dispersive mode gradually deteriorates through band narrowing and the development of a wave vector dependent lifetime. A semiclassical theory for finite-T excitations in gapped spin chains was recently developed by Sachdev and Damle [25]. It relies on Δ/J being a small parameter as is the case for the Haldane phase of spin-1 chains, and in weakly dimerized spin-1/2 chains. In CN the spin gap is instead much greater than the magnetic bandwidth. Our data should provide a focus for theoretical attempts to describe finite temperature properties in this "strong coupling" limit.

It is a pleasure to acknowledge the assistance provided by the staff of the RAL during the measurements, and we thank R. Eccleston for illuminating discussions. We also thank W. Wong-Ng for help on characterizing crystals, and R. Paul for neutron activation analysis at NIST. The work at JHU was supported by the NSF through DMR-9453362 and DMR-9357518. D. H. R. acknowledges support from the David and Lucile Packard Foundation.

[1] I. Affleck, J. Phys. Condens. Matter. **1**, 3047 (1989).
[2] E. Dagotto and T. M. Rice, Science **271**, 618 (1996).
[3] J. C. Bonner *et al.*, J. Appl. Phys. **50**, 1810 (1979).
[4] J. C. Bonner *et al.*, Phys. Rev. B **27**, 248 (1983).
[5] A. W. Garrett *et al.*, Phys. Rev. Lett. **79**, 745 (1997).
[6] J. Eckert *et al.*, Phys. Rev. B **20**, 4596 (1979).
[7] K. M. Diederix *et al.*, Physica (Amsterdam) **94B**, 9 (1978).
[8] B. Morosin, Acta Crystallogr. Sect. B **26**, 1203 (1970).
[9] G. Xu, Ph.D. thesis, The Johns Hopkins University, 1999.
[10] C. J. Carlile and M. A. Adams, Physica (Amsterdam) **182B**, 431 (1992); R. Crevecoeur *et al.*, Nucl. Instrum. Methods Phys. Res., Sect. A **356**, 415 (1995).
[11] P. J. Brown, in *International Tables for Crystallography,* edited by A. J. C. Wilson and E. Prince (Kluwer Academic Publishers, Boston, 1999), Vol. C.
[12] S. W. Lovesey, *Theory of Neutron Scattering from Condensed Matter* (Clarendon, Oxford, 1984).
[13] A. B. Harris, Phys. Rev. B **7**, 3166 (1973); T. Barnes, J. Riera, and D. A. Tennant, *ibid.* **59**, 11 384 (1999).
[14] R. S. Eccleston *et al.*, Phys. Rev. Lett. **81**, 1702 (1998), report a similar effect in $Sr_{14}Cu_{24}O_{41}$.
[15] P. C. Hohenberg and W. F. Brinkman, Phys. Rev. B **10**, 128 (1974).
[16] S. M. Girvin, A. H. MacDonald, and P. M. Platzman, Phys. Rev. B **33**, 2481 (1986).
[17] S. Ma *et al.*, Phys. Rev. Lett. **69**, 3571 (1992).
[18] D. A. Tennant *et al.* (unpublished).
[19] M. Stone *et al.* (unpublished).
[20] B. Leuenberger *et al.*, Phys. Rev. B **30**, 6300 (1984).
[21] Y. Sasago *et al.*, Phys. Rev. B **55**, 8357 (1997).
[22] O. Fritz, S. W. Lovesey, and G. I. Watson, J. Phys. Condens. Matter **10**, 6321 (1998).
[23] M. Matsuda *et al.*, Phys. Rev. B **59**, 1060 (1999).
[24] P. A. Lindgård and B. Schmid, Phys. Rev. B **48**, 13 636 (1993).
[25] S. Sachdev and K. Damle, Phys. Rev. Lett. **78**, 943 (1997).